Journal of Biomolecular NMR (2005) 32: 163–173
DOI 10.1007/s10858-005-5027-3

Article

Off-resonance rotating-frame amide proton spin relaxation experiments measuring microsecond chemical exchange in proteins

Patrik Lundström & Mikael Akke*
Department of Biophysical Chemistry, Lund University, P.O. Box 124, SE-22100, Lund, Sweden

Received 28 February 2005; Accepted 28 March 2005

Key words: conformational exchange, rotating-frame relaxation, spin-lock, calmodulin, EF-hand

Abstract

NMR spin relaxation in the rotating frame ($R_{1\rho}$) is a unique method for atomic-resolution characterization of conformational (chemical) exchange processes occurring on the microsecond time scale. Here, we use amide ^{1}H off-resonance $R_{1\rho}$ relaxation experiments to determine exchange parameters for processes that are significantly faster than those that can be probed using ^{15}N or ^{13}C relaxation. The new pulse sequence is validated using the E140Q mutant of the C-terminal domain of calmodulin, which exhibits significant conformational exchange contributions to the transverse relaxation rates. The ^{1}H off-resonance $R_{1\rho}$ data sample the entire relaxation dispersion profiles for the large majority of residues in this protein, which exchanges between conformations with a time constant of approximately 20 μs. This is in contrast to the case for ^{15}N, where additional laboratory-frame relaxation data are required to determine the exchange parameters reliably. Experiments were performed on uniformly ^{15}N-enriched samples that were either highly enriched in ^{2}H or fully protonated. In the latter case, dipolar cross-relaxation with aliphatic protons were effectively decoupled to first order using a selective inversion pulse. Deuterated and protonated samples gave the same results, within experimental errors. The use of deuterated samples increases the sensitivity towards exchange contributions to the ^{1}H transverse relaxation rates, since dipolar relaxation is greatly reduced. The exchange correlation times determined from the present ^{1}H off-resonance $R_{1\rho}$ experiments are in excellent agreement with those determined previously using a combination of ^{15}N laboratory-frame and off-resonance $R_{1\rho}$ relaxation data, with average values of $\langle\tau_{ex}\rangle = 19 \pm 7$ and 21 ± 3 μs, respectively.

Abbreviations: DSS – 2,2-dimethyl-2-silapentane-5-sulfonic acid; Tr2C – the C-terminal domain of bovine calmodulin (residues 76–148).

Introduction

Nuclear spin relaxation is a powerful method for characterizing biomolecular dynamics. Motions on a wide range of time scales may be studied, from the very rapid fluctuations of bond vectors that take place on picosecond to nanosecond time scales, to slower collective motions in the microsecond to millisecond regime. The latter type of dynamics may be important for enzymatic catalysis (Eisenmesser et al., 2002; Wolf-Watz et al., 2004), ligand binding (Malmendal et al., 1999), and allosteric regulation (Akke, 2002; Palmer, 2004; Yan et al., 2004). These types of processes may be characterized quantitatively using Carr–Purcell–Meiboom–Gill (CPMG) or rotating-frame spin-lock ($R_{1\rho}$) experiments, in which conformational (or chemical) exchange between substates with different chemical shifts is manifested by a dispersion of the

*To whom correspondence should be addressed. E-mail: mikael.akke@bpc.lu.se

transverse relaxation rate as a function of the effective radio-frequency (RF) field strength (Palmer et al., 2001). Typically, the frequency of nutation around the effective field should match the exchange rate of the molecular process studied.

In the past, $R_{1\rho}$ experiments have been used predominantly to characterize motions with time scales on the order of 10–100 μs, where CPMG experiments start to fail due to limitations on the achievable effective field. In addition, recent theoretical and methodological advances have shown that $R_{1\rho}$ experiments are very useful also for significantly slower motions, since all exchange parameters (viz. rates, populations, and chemical shift differences) can be determined at a single static magnetic field strength (Trott and Palmer, 2002; Trott et al., 2003; Korzhnev et al., 2005). The large majority of reports have measured exchange via ^{15}N relaxation dispersion (Akke and Palmer, 1996), but methods have been developed also for the backbone amide ^{1}H (Almeida and Opella, 1997; Ishima et al., 1998), and backbone carbonyl ^{13}C (Mulder and Akke, 2003). The major advantage of ^{15}N is that its relaxation is totally dominated by the dipolar interaction with the covalently attached proton, which contributes approximately 80% of the total auto-relaxation, and by its chemical shift anisotropy (CSA), which contributes 20% (at $B_0 = 11.7$ T), while other mechanisms contribute very little (<1%). The significant cross-relaxation pathways affecting ^{15}N are readily decoupled (Palmer et al., 1992; Kay et al., 1992; Korzhnev et al., 2002; Massi et al., 2004). In addition, the three-bond scalar coupling between backbone ^{15}N spins in adjacent residues is negligible, making coherent magnetization transfer by Hartmann–Hahn matching during the relaxation period highly inefficient. By comparison, Hartmann–Hahn transfer may cause significant problems in relaxation dispersion experiments on ^{1}H and ^{13}C that require careful consideration of the experimental design (Mulder et al., 2002; Mulder and Akke, 2003). The main disadvantage with ^{15}N is its low gyromagnetic ratio, which puts an upper limit on the RF field strengths that can be applied without encountering technical problems, such as probe arcing (Keifer, 1999). The practical limits on RF field strengths currently achievable for ^{13}C and ^{15}N spin-lock experiments are around 5 and 2 kHz, respectively. Since characterization of fast conformational exchange requires high spin-lock field strengths, these limitations impose an upper limit on the exchange rates that are accessible to study. In our experience, quantitative analysis of motional time scales on the order of 20 μs requires additional experimental data besides the ^{15}N $R_{1\rho}$ rates to define the high-frequency limit of the dispersion curve, which corresponds to the exchange-free contribution to R_2, denoted $R_{2,0}$. While $R_{2,0}$ can be estimated readily by measurement of cross-relaxation rates due to interference effects between the ^{15}N CSA and ^{15}N–^{1}H dipolar interactions (Kroenke et al., 1998), it is highly desirable that the $R_{1\rho}$ data in itself sample the entire dispersion profile. In the case of ^{1}H, it is possible to achieve RF field strengths exceeding 10 kHz, which enables full sampling of the dispersion profile for spins that exchange on a time scale on the order of 10 μs. For these reasons, we turned to ^{1}H off-resonance $R_{1\rho}$ experiments (Desvaux et al., 1994, 1995). Here we focus on the relaxation dispersion of backbone amide protons, using ^{15}N-labeled samples to edit the proton spectrum. Previous work along these lines, using on-resonance ^{1}H $R_{1\rho}$ experiments on perdeuterated samples, has mapped out structural regions exhibiting exchange in the HIV-1 protease (Ishima et al., 1998).

The present pulse sequence is validated using the E140Q mutant of the C-terminal domain of calmodulin (M_r 8 kDa), which exhibits significant conformational exchange contributions to the transverse relaxation rates. The calcium-saturated state of E140Q-Tr2C exchanges between conformations that resemble the apo and calcium-saturated states of the wild-type domain (wt-Tr2C), as gauged from the chemical shifts and pattern of NOESY cross-peaks (Evenäs et al., 1997, 1999, 2001). The conformational changes between apo and calcium-saturated wt-Tr2C include extensive repacking of the hydrophobic core, reorientations of the α-helices and exposure of a hydrophobic surface (Chattopadhyaya et al., 1992; Finn et al., 1995; Kuboniwa et al., 1995; Zhang et al., 1995). This conformational switch is essential for binding to a large number of target proteins (Vogel, 1994; Crivici and Ikura, 1995). Measurements of ^{15}N off-resonance $R_{1\rho}$, together with laboratory-frame relaxation data (R_1, R_2, and $R_{2,0}$), on E140Q-Tr2C have revealed that the average exchange correlation time is $\langle\tau_{ex}\rangle = 21$ μs at 28 °C, and that the two dominating populations are approximately equal (Evenäs et al., 2001). The sizeable exchange contribution to the transverse relaxation rates

makes E140Q-Tr2C is a good model system for studying the dynamics of large-scale structural transitions.

Theory and experimental design

Relaxation in the rotating frame

The auto-relaxation rate of a spin magnetization locked in a tilted rotating frame is given by (Cavanagh et al., 1995; Palmer, 2004):

$$R_{1\rho} = R_1 \cos^2\theta + \left(R_{2,0} + R_{\mathrm{ex}}\right)\sin^2\theta \qquad (1)$$

where R_1 is the longitudinal relaxation rate, $R_{2,0}$ and R_{ex} are the exchange-free and exchange contributions to the transverse relaxation rate, respectively, $\theta = \arctan(\omega_1/\Omega)$ is the tilt angle between the static magnetic field and the effective field, with ω_1 being the spin-lock field strength (expressed in frequency units) and Ω being the resonance offset from the carrier frequency. The auto-relaxation rates R_1 and $R_{2,0}$ for spin I can be expressed as linear combinations of spectral densities, according to

$$R_1 = \sum_S \frac{\hbar^2\mu_0^2\gamma_I^2\gamma_S^2}{64\pi^2 r_{IS}^6}\left[J(\omega_I-\omega_S) + 3J(\omega_I) + 6J(\omega_I+\omega_S)\right] + \frac{B_0^2\gamma_I^2\Delta\sigma_I^2}{3}J(\omega_I), \qquad (2)$$

$$R_{2,0} = \sum_S \frac{\hbar^2\mu_0^2\gamma_I^2\gamma_S^2}{128\pi^2 r_{IS}^6}\left[4J(0) + J(\omega_I-\omega_S) + 3J(\omega_I) + 6J(\omega_S) + 6J(\omega_I+\omega_S)\right] + \frac{B_0^2\gamma_I^2\Delta\sigma_I^2}{18}[4J(0)+3J(\omega_I)], \qquad (3)$$

where $J(\omega) = 2/5 \times \tau_c/(1 + \omega^2\tau_c^2)$; $\hbar$ is Planck's constant divided by 2π; μ_0 is the permeability of free space, γ_I and γ_S are the gyromagnetic ratios of spins I and S, r_{IS} is the internuclear distance between the two spins, B_0 is the static magnetic field, and $\Delta\sigma_I$ is the chemical shift anisotropy of an axially symmetric chemical shift tensor.

R_{ex} arises from stochastic modulation of the isotropic chemical shift due to motions slower than overall rotational diffusion. The functional form of R_{ex} depends primarily on the ratio between the rate of exchange, $k_{\mathrm{ex}} = 1/\tau_{\mathrm{ex}}$, and the chemical shift difference between the exchanging states $\Delta\omega$ (Palmer et al., 2001; Palmer, 2004). For fast conformational exchange ($k_{\mathrm{ex}}/\Delta w \gg 1$) between two states A and B, R_{ex} is given by (Davis et al., 1994; Desvaux et al., 1994):

$$R_{\mathrm{ex}} = \frac{\phi_{\mathrm{ex}}\tau_{\mathrm{ex}}}{1+\omega_{\mathrm{eff}}^2\tau_{\mathrm{ex}}^2} \qquad (4)$$

where $\phi_{\mathrm{ex}} = p_A p_B \Delta\omega^2$, p_A and p_B are the populations of the substates, and $\omega_{\mathrm{eff}} = (\omega_1{}^2 + \Omega^2)^{1/2}$ is the effective field strength of the spin-lock. By performing experiments at different effective fields, it is thus possible to characterize the exchange and determine the parameters τ_{ex} and ϕ_{ex}. The lorentzian form of Equation 4 directly shows that high effective fields are required to sample adequately the relaxation dispersion for processes with short values of τ_{ex}.

The rotating-frame cross-relaxation rates σ_{IS} are given by expressions analogous to those for the auto-relaxation rates, Equation 1. The weighting of longitudinal and transverse dipolar cross-relaxation rates ($\sigma_{IS}^{\mathrm{NOE}}$ and $\sigma_{IS}^{\mathrm{ROE}}$, respectively) are given by the product of the projections of each spin operator on their respective alignment axis (Desvaux et al., 1994; Cavanagh et al., 1995):

$$\sigma_{IS} = \sigma_{IS}^{\mathrm{NOE}}\cos\theta_I\cos\theta_S + \sigma_{IS}^{\mathrm{ROE}}\sin\theta_I\sin\theta_S, \qquad (5)$$

$$\sigma_{IS}^{\mathrm{NOE}} = \frac{\hbar^2\mu_0^2\gamma_I^2\gamma_S^2}{64\pi^2 r_{IS}^6}[6J(\omega_I+\omega_S) - J(\omega_I-\omega_S)], \qquad (6)$$

$$\sigma_{IS}^{\mathrm{ROE}} = \frac{\hbar^2\mu_0^2\gamma_I^2\gamma_S^2}{64\pi^2 r_{IS}^6}[2J(\omega_I-\omega_S) + 3J(\omega_I)]. \qquad (7)$$

Dipolar cross relaxation occurs between spin I and all spins S included in the sums of Equations 2 and 3. σ_{IS} constitutes an efficient relaxation pathway when I and S have the same gyromagnetic ratio, such that $J(\omega_I - \omega_S) \approx J(0)$, and particularly for nuclides with high γ, such as protons.

The effect of cross relaxation

The amide proton $R_{1\rho}$ pulse sequence used here is shown in Figure 1. The experiment is essentially a

^{15}N-filtered ^{1}H ROESY, in which the spin system evolves during the relaxation delay according to

$$\mathbf{I}(t) = \exp[-\mathbf{R}t_{\mathrm{SL}}]\mathbf{I}(0), \tag{8}$$

where $\mathbf{I}(t)$ is the magnetization vector and $\mathbf{R}$ is the relaxation matrix, with diagonal elements R_{ii} given by Equation 1, and off-diagonal elements R_{ij} given by Equation 5. Thus, relaxation is multi-exponential in general due to cross relaxation within the network of coupled protons. However, for sufficiently short spin-lock relaxation delays, such that $R_{ij}R_{jk}t_{SL}^2 \ll 1$, both auto- and cross-relaxation are mono-exponential, and the latter includes only single magnetization transfer steps between pairs of spins. In the present experiment (Figure 1), the amide proton magnetizations relax as diagonal peaks in a ROESY spectrum (Desvaux et al., 1994; Ishima et al., 1998), and ROESY-type cross peaks build up during the spin-lock period (Desvaux et al., 1994). Magnetization transfer to non-amide protons is greatly reduced in highly deuterated protein samples. In contrast, cross relaxation between amide protons still remains in perdeuterated samples. It is thus essential to verify that cross relaxation does not introduce any significant errors in the extracted relaxation rates. We performed model calculations based on internuclear distances in regular secondary structure elements including the amide nitrogen and proton and additional amide protons within 5 Å. For α-helices this includes H^N_{i+1}, H^N_{i+2}, and H^N_{i+3}, with interproton distances of 2.70, 4.16, and 4.70 Å, respectively, as calculated from the average coordinates of the helical residues in the C-terminal domain of calcium-loaded calmodulin (pdb id: 1J7P; Chou et al., 2001). For β-sheets the distance to the closest amide proton shows significant variation, but in general it is

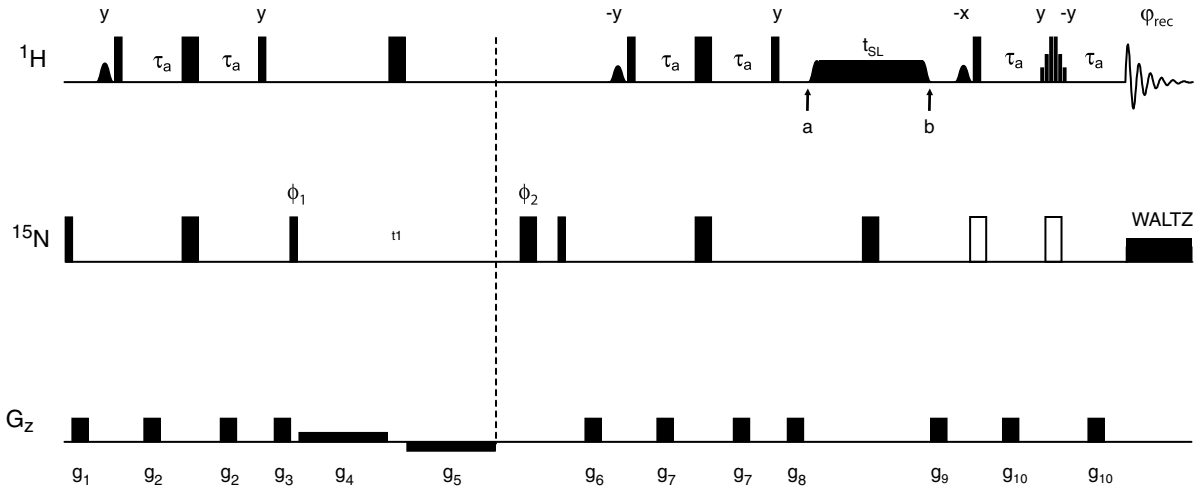

Figure 1. Pulse sequence used to measure ^{1}H $R_{1\rho}$. Narrow and wide bars indicate 90° and 180° pulses, respectively. All pulses are applied with phase x unless otherwise indicated. All ^{1}H pulses are applied with the carrier frequency centered on the water resonance, except for between time points a and b when it is moved to the desired offset. Low power pulses are used to excite the water resonance selectively, and are given as rectangular pulses with a field strength of $\gamma B_1/2\pi$ = 125 Hz. The phase of these pulses should be fine-tuned to optimize water suppression. The final element is a 3-9-19 binomial WATERGATE sequence (Sklenar et al., 1993). ^{15}N pulses are centered at 119 ppm. ^{15}N-decoupling during acquisition employs the WALTZ-16 sequence (Shaka et al., 1983) with a field strength of $\gamma B_1/2\pi$ = 1100 Hz. The phase cycle is $\phi_1 = x,-x$; $\phi_2 = x,x,y,y,-x,-x,-y,-y$; $\phi_{\mathrm{rec}} = x,-x,-x,x$. Quadrature detection in t_1 is obtained by the States-TPPI method (Marion et al., 1989). The spin-echo following t_1 allows for an initial sampling delay of zero. The INEPT refocusing delay was set to $2\tau_a = 1/(2J_{\mathrm{NH}})$. Gradient strengths (G cm^{-1}), lengths (ms): $g1$ = 15,000 (1.0), $g2$ = 6000 (1.0), $g3$ = 15,000 (1.0), $g4 = -g5$ = 500 (t_1/2), $g6$ = 11,000 (1.0), $g7$ = 6000 (0.5), $g8$ = 7000 (1.0), $g9$ = −13,000 (1.0), and $g10$ = 19,000 (0.9). Heat compensation is achieved using continuous wave radiation, applied far off-resonance prior to the first pulse of the sequence (not shown) (Wang and Bax, 1993). A 90_x-180_y-90_x composite 180° pulse is applied on ^{13}C in the middle of t_1 in order to refocus scalar couplings to C′ and C$^{\alpha}$ (not shown). This pulse was centered at 119 ppm and had a field strength of $\gamma B_1/2\pi$ = 8800 Hz, which gives 98% inversion at 58 and 176 ppm. Filled bars indicate the basic pulse sequence, while open bars represent optional pulses that may be included to implement TROSY type detection (Pervushin et al., 1997). In this case, two separate experiments are recorded: one that includes the 180° pulses represented by open rectangles, and one that does not include any pulses on ^{15}N from point a to the end of the sequence. The resulting spectra are added/subtracted to select the slowly relaxing component (Ottiger et al., 1998).

larger than in the case of helices. The protein was assumed to be rigid with isotropic rotational diffusion. Calculations were performed as a function of τ_c; for each value of τ_c, the maximal relaxation delay was adjusted so as to monitor the decay to the same extent as in the present work (see below). The numerical calculations show that the mono-exponential approximation of the decay results in relative errors in extracted rates, $\varepsilon(R_{1\rho})$, as follows. In the limit $\theta = 0$, the error scales approximately linearly with τ_c: $\varepsilon(R_{1\rho}) \approx 0.01\tau_c/10$ ns, over a range from $\tau_c = 0$–20 ns; at longer correlation times, $\varepsilon(R_{1\rho})$ levels off towards a constant value of 2.5% at the point where the ^1H–^1H dipolar contribution to R_1 starts to dominate over the dipolar interactions with ^{15}N, such that auto- and cross-relaxation both increase linearly with τ_c. In the limit $\theta = 90°$, $\varepsilon(R_{1\rho})$ reaches a plateau of 0.7% at $\tau_c = 10$ ns. Thus, $\varepsilon(R_{1\rho}) < 3\%$ for any tilt angle and τ_c. However, for increasing values of τ_c, complications arise due to overlap between ROESY-type cross-peaks and auto peaks, and by increasingly faster relaxation. In the case of E140Q-Tr2C, $\varepsilon(R_{1\rho}) < 0.5\%$ for both helices and sheets, in the case of on-resonance spin-locks. The error will be smaller if the spin is relaxed additionally by conformational exchange. In the case of spin-lock fields applied far off resonance, the error will be less than 0.3% and essentially independent of conformational exchange. Inclusion of additional spins in the model does not alter the results significantly, due to the strong distance dependence of the dipolar interaction.

Cross correlations between the ^{15}N–^1H dipolar and ^1H CSA interactions, and between ^{15}N–^1H and ^1H–^1H dipolar interactions, lead to cross relaxation between in-phase ($H_{x,y}$) and anti-phase operators ($H_{x,y}N_z$). These interference effects are suppressed by inverting the ^{15}N dipolar field in the middle of the relaxation delay (Palmer et al., 1992; Kay et al., 1992). The ^1H–^2H dipolar interaction is 6% of that between protons, making auto- and cross-correlated mechanisms involving these spins insignificant.

In cases where deuteration is not feasible, cross relaxation involving aliphatic protons may still be effectively decoupled if a selective 180° pulse is applied on the aliphatic or amide protons at the mid-point of the relaxation period. Inversion of the aliphatic protons is preferred, since it also suppresses cross correlation between the ^1H CSA and ^1H–^1H dipolar interactions involving aliphatic spins. In combination with the use of short relaxation delays, this approach achieves effective suppression of cross relaxation. However, the high auto-relaxation rate in protonated samples causes a loss in overall sensitivity.

The effect of Hartmann-Hahn magnetization transfer

The efficiency of Hartmann–Hahn coherence transfer is given by (van de Ven, 1995):

$$F = \frac{1}{1 + (\Delta/J_{\mathrm{eff}})^2} \sin^2(Dt_{\mathrm{SL}}/2), \qquad (9)$$

where $D = (\Delta^2 + J_{\mathrm{eff}}{}^2)^{1/2}$, $\Delta = \omega_{\mathrm{effI}} - \omega_{\mathrm{effS}}$ is the mismatch, $\omega_{\mathrm{effi}} = (\omega_1{}^2 + \Omega_i{}^2)^{1/2}$ is the effective field strength experienced by spin i, $J_{\mathrm{eff}} = J[1 + \cos(\theta_I - \theta_S)]/2$ the effective coupling constant, J the scalar coupling constant, and t_{SL} is the relaxation delay (corresponding to the "mixing time"). Given the parameters of the present continuous-wave spin-lock experiments (see below), Hartmann–Hahn transfer is inefficient between the amide and alpha protons, as long as the spin-lock carrier is placed in the center, or downfield, of the amide region. The maximum amplitude of F encountered in the present study is less than 2% in the case of a fully protonated sample, and is completely negligible for the large majority of spins.

Materials and methods

Sample preparation

Highly deuterated (approximately 85%) and uniformly $^{13}C/^{15}N$-enriched E140Q-Tr2C was obtained by over-expression in *Escherichia coli* MM294 using ^{13}C-glucose and $^{15}NH_4Cl$ as the sole carbon and nitrogen sources, and 97% D_2O in the culture medium. The NMR sample consisted of 1.5 mM protein dissolved in 90%/10% H_2O/D_2O containing 20 equivalents of calcium, 100 μM 2,2-dimethyl-2-silapentane-5-sulfonic acid (DSS) and 200 μM NaN_3. The pH was set to 6.0. Under these conditions, the calcium-saturated state is populated to >98% (Evenäs et al., 1997).

NMR spectroscopy

All experiments were performed on a Varian INOVA spectrometer operating at a ^{1}H Larmor frequency of 499.86 MHz. The temperature was set to 27.1°C to obtain a nominal temperature of 28°C during the spin-lock experiments. The temperature was calibrated by measuring the frequency difference between the DSS and solvent resonances. Heat compensation pulses were implemented as described (Wang and Bax, 1993) to avoid differential heating for different RF field strengths and relaxation delays. In all experiments, 128 and 512 complex points were recorded in t_1 and t_2, respectively. The recycle delay was 1 s.

Amide ^{1}H $R_{1\rho}$ rate constants were measured using the pulse sequence shown in Figure 1. Briefly, the pulse sequence consists of an INEPT polarization transfer step, ^{15}N chemical shift evolution during t_1, a reverse INEPT transfer, a ^{1}H spin-lock relaxation period of total length t_{SL}, and a WATERGATE scheme (Sklenar et al., 1993), followed by ^{1}H detection during t_2. The spin-lock relaxation period was bracketed by tan/tanh adiabatic sequences (Garwood and Ke, 1991; Ugurbil et al., 1988) to align the magnetizations with their respective effective fields (Mulder et al., 1998). The tan/tanh adiabatic pulses had durations of 4 ms, and the frequency sweep was initiated at 25 kHz from the spin-lock carrier frequency. The data were recorded in fully interleaved fashion as four-dimensional arrays, where the first and second dimensions correspond to the t_1 and t_2 evolution periods, the third dimension to the relaxation delay t_{SL}, and the fourth to either the spin-lock field strength ω_1, or offset Ω. On-resonance experiments were performed with the carrier placed at 8.0 ppm and RF field strengths of 3041, 3401 3864, 4237, 4808, 5435, 6219, 6667, 7752, 8621, 9842, 10864, 12136, and 13587 Hz; with the carrier placed at 8.5 ppm and RF field strengths of 1053 and 1938 Hz; or with the carrier placed at 7.5, 8.5, 9.0, or 10.0 ppm and a field strength of 602 Hz. Off-resonance experiments used a constant RF spin-lock field strength of $\omega_1/2\pi = 9842$ Hz and and 12 different offsets ranging from 1 to 24 kHz, corresponding to a range of ω_{eff} from $1.4\omega_1$ to $2.6\omega_1$. In addition, two offsets of 50 and 200 kHz were included to sample the dispersion curve at small tilt angles (down to $\theta = 3°$). Spin-lock field strengths were measured as the inverse of the 360°-pulse length. For each effective field strength, the decay was sampled between 0 and 30 ms, using six to ten data points, including duplicates. The experiment was repeated on a fully protonated sample using similar RF field strengths and offsets. For these experiments, band-selective inversion was applied to the amide protons in the middle of the relaxation delay using a 1990 μs I-BURP pulse centered at 9 ppm (Geen and Freeman, 1991). The amide ^{1}H magnetization was returned to the z-axis and the spin-lock field was turned off prior to the I-BURP pulse; subsequently, the amide ^{1}H magnetization was realigned with the effective field and spin-locking resumed.

Data processing and analysis

All data were processed using nmrPipe (Delaglio et al., 1995). The data were apodized in t_1 and t_2 with cosine and lorentzian-to-gaussian window functions, respectively, and zero filled to 512 and 4096 points prior to Fourier transformation. Peak intensities were measured by summing 3×5 ($t_1 \times t_2$) points centered on the peak maximum. Extraction of $R_{1\rho}$ decay rates and exchange parameters was performed using in-house software employing the Levenberg–Marquardt algorithm (Press et al., 1988). Mono-exponential functions were fitted to the decays at each tilt angle. The $R_{1\rho}$ dispersion curves were fitted using both a 2-parameter model that included R_1 and $R_{2,0}$, corresponding to Equation 1 with $R_{ex} = 0$, and a 4-parameter model that included R_1, $R_{2,0}$, τ_{ex}, and ϕ_{ex}, corresponding to Equations 1 and 4. F-tests were used to determine the appropriate model; $p < 0.05$ was considered significant. The 4-parameter model was also rejected if the uncertainty in the fitted parameters exceeded the parameter values. Global optimization of τ_{ex} was achieved using simulated annealing (Press et al., 1988). Errors in fitted parameters were estimated by the Monte–Carlo procedure (Press et al., 1988), using 1000 synthetic data sets.

Results and discussion

The experimental scheme for measuring ^{1}H $R_{1\rho}$ relaxation rate constants is shown in Figure 1. This pulse sequence is based on previous methods reported by Ishima et al. (1998). Our approach

incorporates off-resonance $R_{1\rho}$ measurements, which significantly extend ω_{eff} towards higher field strengths, and hence enable studies of faster exchange processes. In addition, the present pulse sequence includes modifications to improve restoration of the water magnetization along the positive z-axis, resulting in excellent solvent suppression.

Significant auto relaxation, as observed in fully protonated samples, reduces the sensitivity of relaxation dispersion experiments towards exchange. Methods for mitigating this problem have been presented, including constant relaxation time strategies (Akke and Palmer, 1996; Wang et al., 2001), TROSY-based detection (Ishima et al., 1998), and combinations thereof (Kempf et al., 2003). In the present case, the optional TROSY scheme (Figure 1) is unfavorable, due to the relatively low molecular weight of E140Q-Tr2C and the nominal reduction in sensitivity by a factor of $2^{1/2}$

Figure 2 shows the effect of cross relaxation for a protonated sample. Build-up of ROESY-and NOESY-type cross-peaks is evident at large and small tilt angles, respectively (Figure 2a and b). As shown by Equations 5–7, the opposite sign of σ^{ROE} and σ^{NOE} results in cancellation of cross-relaxation at $\theta = 35°$ (Figure 2C). In principle, it is therefore possible to perform ^{1}H $R_{1\rho}$ dispersion experiments without any complications due to cross-relaxation by varying the spin-lock field strength while maintaining the tilt angle at 35° (Desvaux et al., 1995). However, in practice it is not possible to achieve satisfactory alignment of all spins at $\theta = 35°$ simultaneously, using low effective fields. Furthermore, using a constant value of $\theta = 35°$, the sensitivity to exchange is reduced by a factor of $\sin^2(35°) = 0.33$. For these reasons, we prefer to suppress cross-relaxation in protonated samples by applying a band-selective inversion pulse to the amide protons, as shown in Figure 2D. Cross-relaxation is further minimized by using short relaxation delays as discussed above.

We obtained relaxation dispersion data for 59 out of the 73 residues of E140Q-Tr2C. Data for the remaining residues could not be extracted reliably due to either spectral overlap or severe line broadening. Figure 3 shows representative $R_{1\rho}$ decays at two different tilt angles. As can be seen, the decays are well represented by mono-exponential functions. To determine the parameters R_1, $R_{2,0}$, ϕ_{ex}, and τ_{ex}, we measured $R_{1\rho}$ at 31 different effective fields (Figure 4). For 17 of

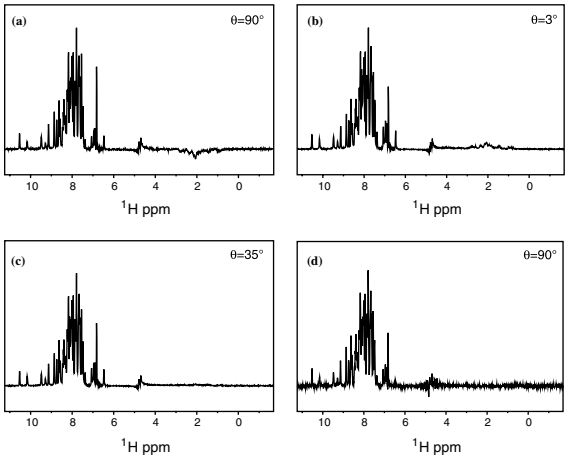

Figure 2. One-dimensional spectra showing the effects of cross relaxation in the ^{1}H $R_{1\rho}$ sequence applied to a protonated sample. Spectra are shown for tilt-angles of (A) 90°, (B) 3°, (C) 35°, and (D) 90°. Spectra A–C were acquired using the pulse sequence shown in Figure 1, while spectrum D was acquired with a band-selective inversion pulse applied to the aliphatic protons in the middle of the relaxation delay. ROESY and NOESY type cross-peaks are clearly visible in spectra A and B, respectively, while cross relaxation is effectively eliminated in C, cf. Equation 5. Spectrum D illustrates the efficient cancellation of cross relaxation between amide and aliphatic protons achieved by inverting the former at $t_{SL}/2$. The lower signal-to-noise ratio in D is due to reduced signal averaging (eight transients, as compared to 128 for the other spectra).

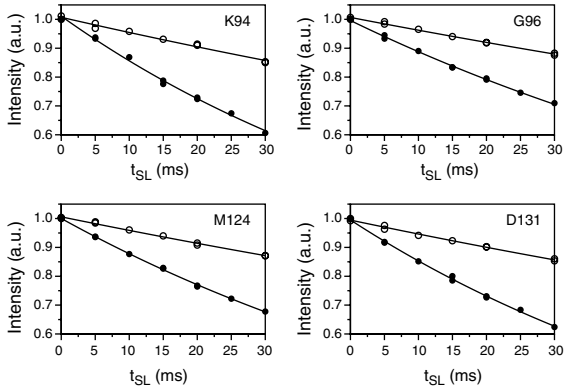

Figure 3. Representative $R_{1\rho}$ relaxation decays obtained using a spin-lock field strength of $\omega_1 = 9842$ Hz and nominal offsets of $\Omega = 0$ Hz (filled circles) and 18 kHz (open circles). The different panels show data for different residues, as indicated: K94, G96, M124, and D131. The lines represent the best fit of mono-exponential functions to the data. The estimated error in intensity is approximately of the same the size as the symbols.

those, the spin-lock field was positioned at 8.0 ppm and the field strength was varied from 602 to 13587 Hz. Previous ^{15}N $R_{1\rho}$ experiments have shown that τ_{ex} is approximately 20 μs (Evenäs et al., 2001). Consequently, the present range of effective fields achieved with the carrier positioned on resonance suffices to sample the dispersion curve from a point very close to the free precession limit ($\omega_{eff} = 0$) to points well beyond the inflection point at $\omega_{eff}/2\pi \approx 8$ kHz. Including 12 off-resonance data points with effective field strengths in the range $\omega_{eff}/2\pi$ = 10–26 kHz (corresponding to tilt angles of θ = 84–22°), the ^{1}H $R_{1\rho}$ data alone is sufficient to define the entire relaxation dispersion curve for the large majority of residues, Figure 4. This is in contrast to the ^{15}N $R_{1\rho}$ experiments applied to E140Q-Tr2C, which need to be supplemented with additional relaxation data, e.g., $R_{2,0}$, obtained from separate experiments. Figure 4A shows the $R_{1\rho}$ rates plotted vs. the tilt angle for the same residues as in Figure 3. The existence of conformational exchange is clearly identified from variation with ω_1 of the on-resonance $R_{1\rho}$ rates (around θ = 90°), as exemplified by residues K94 and D131. In the absence of conformational exchange, the on-resonance $R_{1\rho}$ rates should not vary, provided that the small difference in tilt angles for different field strengths may be neglected, as exemplified by residues G96 and M124 (Figure 4A). Quantitative analyses involving *F*-tests were performed to determine whether a given residue was best represented by a model including or excluding conformational exchange. We identified conformational exchange for 32 of the 59 residues analyzed (Figure 5). The average time constant was $\langle\tau_{ex}\rangle = 19 \pm 7$ μs, which is in excellent agreement with the previous result $\langle\tau_{ex}\rangle = 21 \pm 3$ μs, obtained from ^{15}N $R_{1\rho}$ dispersion data (Evenäs et al., 2001). For the protonated sample the average time constant was $\langle\tau_{ex}\rangle = 22 \pm 4$ μs. This result verifies that the exchange is fast on the chemical shift time scale, in agreement with previous results from B_0-dependent ^{15}N–^{1}H multiple-quantum relaxation experiments (Lundström and Akke, 2004). From the determined parameters R_1, $R_{2,0}$, τ_{ex}, and ϕ_{ex}, we calculated R_2 as a function of ω_{eff}, resulting in the dispersion curves shown in Figure 4B. As expected from Figure 4A, the relaxation dispersion due to conformational exchange is readily

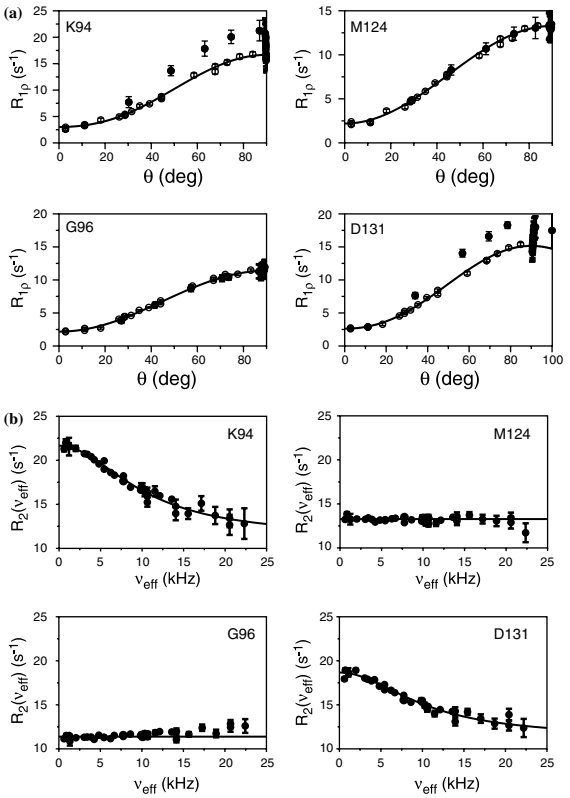

Figure 4. Representative relaxation–dispersion curves. (A) $R_{1\rho}$ plotted as a function of the tilt angle. Filled circles represent data recorded with different spin-lock fields covering the range $\omega_1/2\pi$ = 602–13587 Hz, and with the spin-lock carrier positioned at 8.0 ppm. Open circles represent data recorded with $\omega_1/2\pi$ = 9842 Hz, and different nominal spin-lock carrier offsets covering the range $\Omega/2\pi$ = 1–200 kHz. Note that $R_{1\rho}$ obtained at a given θ will depend on the B_1 field strength for those residues that experience exchange, viz. K94 and D131. Thus, the different data points (filled circles) at θ = 90° and the differences between filled and empty circles at lower θ reflect the dependence of $R_{1\rho}$ on ω_{eff} in the presence of exchange. The fitted line is plotted using $\omega_1/2\pi$ = 9842 Hz, and includes conformational exchange for residues K94 and D131, but not for G96 and M124. Tilt angles greater than 90° occur whenever the adiabatic frequency sweep passes through the offset of a given resonance, such that the effective field has a component along the negative *z*-axis. The resulting data points are equivalent to those obtained with the effective field vector reflected in the *x*–*y* plane. (B) R_2 plotted as a function of the effective field strength. R_2 was calculated from the $R_{1\rho}$ data: $R_2 = R_{1\rho}/\sin^2\theta - R_1/\tan^2\theta$. Due to the increasing uncertainty in R_2 with decreasing θ, only effective field strengths with $W_{eff}/2\pi < 25$ kHz ($\theta > 40°$) are shown here; data obtained at smaller tilt angles primarily serve to determine R_1. The variation in the size of the error bars arises in part because the relaxation decays were sampled with varying numbers (6–10) of data points.

detected for K94 and D131. In contrast, residues G96 and M124 are not subject to exchange, as verified by *F*-tests.

Simultaneous optimization of a global τ_{ex} together with the three residue-specific parameters R_1, $R_{2,0}$, and ϕ_{ex} yielded $\tau_{ex} = 19 \pm 1$ μs (20 ± 1 μs for the protonated sample), which agrees very well with the value of 23 ± 1 μs, obtained from a global fit to the ^{15}N $R_{1\rho}$ data. For half of the residues (16 out of 32), the globally determined τ_{ex} represents the data better than the results from residue-specific optimizations, as gauged by *F*-tests; the remaining 16 residues have significantly lower residuals in the residue-specific fits of τ_{ex}. The residue-specific τ_{ex} values range between 8 and 42 μs and display a relatively minor site-to-site variability (Kroenke et al., 1998; Evenäs et al., 2001) of 9 μs. Together, these results indicate that the conformational exchange is dominated by a global two-state process, with minor contributions from additional states (Evenäs et al., 2001). The simplest model that can account for this observation is three-site exchange involving a sparsely populated intermediate state (Grey et al., 2003; Korzhnev et al., 2004).

As mentioned above, it is not possible to separate the populations from the chemical shift differences in the present case, since the exchange is fast on the chemical shift time scale. The NOESY cross peak patterns and chemical shifts of E140Q-Tr2C indicate that the populations of the two major states are approximately equal (Evenäs et al., 1999, 2001). Assuming equal populations and global two-site exchange, we calculated the magnitude of the chemical shift differences, $|\Delta\delta|$, from ϕ_{ex}. These may be compared with the observed chemical shift differences, $\Delta\delta_{obs}$, between the apo and calcium-loaded states of wild-type Tr2C, as shown in Figure 5B. Linear regression of $|\Delta\delta|$ vs. $\Delta\delta_{obs}$ yields a correlation coefficient of $r_c = 0.45$ ($n = 32$). Previous work has revealed a significant correlation between $|\Delta\delta|$ and $\Delta\delta_{obs}$ for ^{15}N, with $r_c = 0.66$ (Evenäs et al., 2001). Similarly, the product of ^{1}H and ^{15}N chemical shift differences, obtained from ^{1}H–^{15}N multiple-quantum relaxation data, correlate reasonably well, with $r_c = 0.57$ (Lundström and Akke, 2004). Together, these results indicate that the proton chemical shifts are more sensitive to small deviations in conformation of the exchanging states of E140Q-Tr2C from the structures of the apo and calcium-loaded wild-type protein. This may be expected because the ^{15}N chemical shift reports mainly on local backbone dihedral angles (ψ_{i-1}, ϕ_i, and ψ_i), as well as the sidechain χ_1 dihedral angle of the residue itself and the preceeding residue ($i - 1$), and hydrogen bonding (Le and Oldfield, 1994; Xu and Case, 2002). In contrast, the amide ^{1}H chemical shift is not particularly sensitive to local secondary structure, but is often dominated by hydrogen bonds and long-range effects, such as ring-currents and electrostatics (Wishart and Case, 2001). Against this background, the estimated ^{1}H and ^{15}N chemical shift differences between the

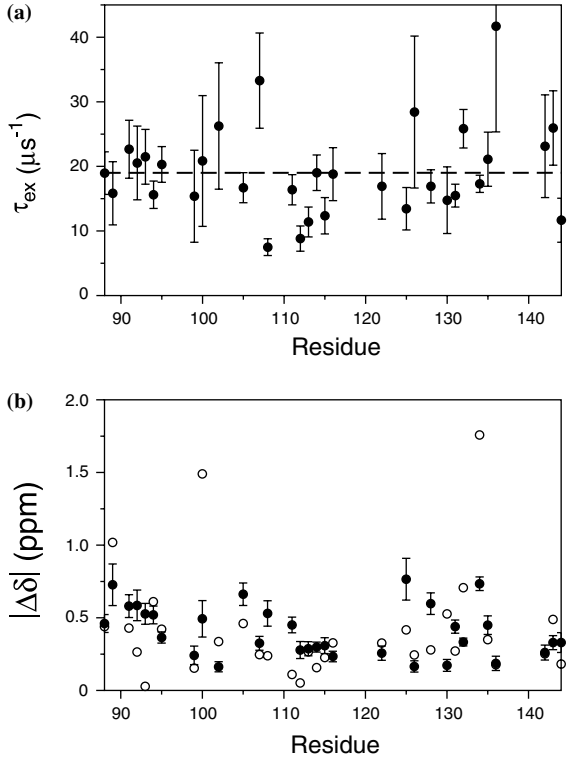

Figure 5. Exchange parameters obtained for E140Q-Tr2C from fits to the $R_{1\rho}$ dispersion curves. (A) Exchange time constants plotted vs. residue number. Results are shown only for those residues where the four-parameter model resulted in a statistically significant improvement in the fit ($p < 0.05$), compared to the two-parameter model, as assessed by the *F*-test (Devore, 1999). The dashed line represents the globally optimized exchange time constant. (B) Chemical shift differences between the exchanging states plotted vs. residue number. Values of $\Delta\delta = \Delta\omega/\gamma B_0$ were calculated from the optimized parameter ϕ_{ex}, obtained from the residue-specific fits, assuming $p_A = p_B$ (filled circles), and from the observed chemical shift differences between the apo- and $(Ca^{2+})_2$-states of wild-type Tr2C (open circles).

exchanging states in E140Q-Tr2C suggest that these resemble the open and closed states of the wild-type protein in terms of secondary structure and hydrogen bonding, but that the detailed packing of aromatic side chains may differ. The present results emphasize the advantage of performing multinuclear relaxation dispersion measurements to obtain complementary information on the underlying conformational exchange process and the conformations involved.

In conclusion, we have presented an experiment that extends the range of time scales that can be characterized completely by $R_{1\rho}$ dispersions. The ^{1}H off-resonance $R_{1\rho}$ data sample the entire relaxation dispersion profiles for the large majority of residues in E140Q-Tr2C, and exchange parameters can be fitted without relying on additional relaxation data, such as estimates of $R_{2,0}$. The exchange correlation times determined from the present ^{1}H off-resonance $R_{1\rho}$ experiments are in excellent agreement with those determined previously using a combination of ^{15}N laboratory-frame and off-resonance $R_{1\rho}$ relaxation data. The experimental data thus verify model calculations showing that cross relaxation with other amide protons leads to only marginal errors in the measured $R_{1\rho}$ for a small protein, such as the C-terminal domain of calmodulin. Moreover, using a simple scheme to suppress cross-relaxation with aliphatic protons, accurate measurements can be obtained also on fully protonated samples.

Acknowledgements

We thank Eva Thulin for protein expression and purification, and Frans Mulder for helpful discussions. This work was supported by research grants from the Swedish Research Council and the Swedish Foundation for Strategic Research, and instrumentation grant from the Knut and Alice Wallenberg Foundation, awarded to M.A.

References

Akke, M. (2002) *Curr. Opin. Struct. Biol.*, **12**, 642–647.
Akke, M. and Palmer, A.G. (1996) *J. Am. Chem. Soc.*, **118**, 911–912.
Almeida, F.C.L. and Opella, S.J. (1997) *J. Magn. Reson.*, **124**, 509–511.
Cavanagh, J., Fairbrother, W.J., Palmer, A.G. and Skelton, N.J., (1995) Protein NMR Spectroscopy: Principles and Practice, Academic Press, San Diego.
Chattopadhyaya, R., Meador, W.E., Means, A.R. and Quiocho, F.A. (1992) *J. Mol. Biol.*, **228**, 1177–1192.
Chou, J.J., Li, S.P., Klee, C.B. and Bax, A. (2001) *Nat. Struct. Biol.*, **8**, 990–997.
Crivici, A. and Ikura, M. (1995) *Ann. Rev. Biophys. Biomol. Struct.*, **24**, 85–116.
Davis, D.G., Perlman, M.E. and London, R.E. (1994) *J. Magn. Reson.*, **B104**, 266–275.
Delaglio, F., Grzesiek, S., Vuister, G.W., Zhu, G., Pfeifer, J. and Bax, A. (1995) *J. Biomol. NMR*, **6**, 277–293.
Desvaux, H., Berthault, P., Birlirakis, N. and Goldman, M. (1994) *J. Magn. Reson.*, **A108**, 219–229.
Desvaux, H., Birlirakis, N., Wary, C. and Berthault, P. (1995) *Mol. Phys.*, **86**, 1059–1073.
Devore J.L., (1999) Probability and Statistics for Engineering and the Sciences, Brooks/Cole Publishing Company, Monterey.
Eisenmesser, E.Z., Bosco, D.A., Akke, M. and Kern, D. (2002) *Science*, **295**, 1520–1523.
Evenäs, J., Forsén, S., Malmendal, A. and Akke, M. (1999) *J. Mol. Biol.*, **289**, 603–617.
Evenäs, J., Malmendal, A. and Akke, M. (2001) *Structure*, **9**, 185–195.
Evenäs, J., Thulin, E., Malmendal, A., Forsén, S. and Carlström, G. (1997) *Biochemistry*, **36**, 3448–3457.
Finn, B.E., Evenäs, J., Drakenberg, T., Waltho, J.P., Thulin, E. and Forsén, S. (1995) *Nat. Struct. Biol.*, **2**, 777–783.
Garwood, M. and Ke, Y. (1991) *J. Magn. Reson.*, **94**, 511–525.
Geen, H. and Freeman, R. (1991) *J. Magn. Reson.*, **93**, 93–141.
Grey, M.J., Wang, C. and Palmer, A.G. (2003) *J. Am. Chem. Soc.*, **125**, 14324–14335.
Ishima, R., Wingfield, P.T., Stahl, S.J., Kaufman, J.D. and Torchia, D.A. (1998) *J. Am. Chem. Soc.*, **120**, 10534–10542.
Kay, L.E., Nicholson, L.K., Delagio, F., Bax, A. and Torchia, D.A. (1992) *J. Magn. Reson.*, **97**, 359–375.
Keifer, P.A. (1999) *Conc. Magn. Reson.*, **11**, 165–180.
Kempf, J.G., Jung, J.Y., Sampson, N.S. and Loria, J.P. (2003) *J. Am. Chem. Soc.*, **124**, 12064–12065.
Korzhnev, D.M., Orekhov, V.Y. and Kay, L.E. (2005) *J. Am. Chem. Soc.*, **127**, 713–721.
Korzhnev, D.M., Salvatella, X., Vendruscolo, M., Di Nardo, A.A., Davidson, A. R., Dobson, C.M. and Kay, L.E. (2004) *Nature*, **430**, 586–590.
Korzhnev, D.M., Skrynnikov, N.R., Millet, O., Torchia, D.A. and Kay, L.E. (2002) *J. Am. Chem. Soc.*, **124**, 10743–10753.
Kroenke, C.D., Loria, J.P., Lee, L.K., Rance, M. and Palmer, A.G. (1998) *J. Am. Chem. Soc.*, **120**, 7905–7915.
Kuboniwa, H., Tjandra, N., Grzesiek, S., Ren, H., Klee, C.B. and Bax, A. (1995) *Nat. Struct. Biol.*, **2**, 768–776.
Le, H. and Oldfield, E. (1994) *J. Biomol. NMR*, **4**, 341–348.
Lundström, P. and Akke, M. (2004) *J. Am. Chem. Soc.*, **126**, 928–935.
Malmendal, A., Evenäs, J., Forsén, S. and Akke, M. (1999) *J. Mol. Biol.*, **293**, 883–899.
Marion, D., Ikura, M., Tschudin, R. and Bax, A. (1989) *J. Magn. Reson.*, **85**, 393–399.
Massi, F., Johnson, E., Wang, C., Rance, M. and Palmer, A.G. (2004) *J. Am. Chem. Soc.*, **126**, 2247–2258.
Mulder, F.A.A. and Akke, M. (2003) *Magn. Reson. Chem.*, **41**, 853–865.

Mulder, F.A.A., de Graaf, R.A., Kaptein, R. and Boelens, R. (1998) *J. Magn. Reson.*, **131**, 351–357.
Mulder, F.A.A., Hon, B., Mittermaier, A., Dahlquist, F.W. and Kay, L.E. (2002) *J. Am. Chem. Soc.*, **124**, 1443–1451.
Ottiger, M., Delaglio, F. and Bax, A. (1998) *J. Magn. Reson.*, **131**, 373–378.
Palmer, A.G. (2004) *Chem. Rev.*, **104**, 3623–3640.
Palmer, A.G., Kroenke, C.D. and Loria, J.P. (2001) *Methods Enzymol.*, **339**, 204–238.
Palmer, A.G., Skelton, N.J., Chazin, W.J., Wright, P.E. and Rance, M. (1992) *Mol. Phys.*, **75**, 699–711.
Pervushin, K., Riek, R., Wider, G. and Wüthrich, K. (1997) *Proc. Natl. Acad. Sci. USA*, **94**, 12366–12371.
Press W.H., Flannery B.P., Teukolsky S.A. and Vetterling W.T. (1988) Numerical Recipes in C. The Art of Scientific Computing Cambridge University Press Cambridge.
Shaka, A.J., Keeler, J. and Freeman, R. (1983) *J. Magn. Reson.*, **53**, 313–340.
Sklenar, V., Piotto, M., Leppik, R. and Saudek, V. (1993) *J. Magn. Reson.*, **A102**, 241–245.
Trott, O., Abergel, D. and Palmer, A.G. (2003) *Mol. Phys.*, **101**, 753–763.
Trott, O. and Palmer, A.G. (2002) *J. Magn. Reson.*, **154**, 157–160.
Ugurbil, K., Garwood, M. and Rath, A.R. (1988) *J. Magn. Reson.*, **80**, 448–469.
van de Ven, F.J.M. (1995) Multidimensional NMR in liquids. Basic Principles and Experimental Methods Wiley-VCH, New York.
Vogel, H.J. (1994) *Biochem. Cell Biol.*, **72**, 357–376.
Wang, A.C. and Bax, A. (1993) *J. Biomol. NMR*, **3**, 715–720.
Wang, C.Y., Grey, M.J. and Palmer, A.G. (2001) *J. Biomol. NMR*, **21**, 361–366.
Wishart, D.S. and Case, D.A. (2001) *Methods Enzymol.*, **338**, 3–34.
Wolf-Watz, M., Thai, V., Henzler-Wildman, K., Hadjipavlou, G., Eisenmesser, E. Z. and Kern, D. (2004) *Nat. Struct. Mol. Biol.*, **11**, 945–949.
Xu, X.P. and Case, D.A. (2002) *Biopolymers*, **65**, 408–423.
Yan, J., Liu, Y., Lukasik, S.M., Speck, N.A. and Bushweller, J.H. (2004) *Nat. Struct. Mol. Biol.*, **11**, 901–906.
Zhang, M., Tanaka, T. and Ikura, M. (1995) *Nat. Struct. Biol.*, **2**, 758–767.